Freie Universität Berlin

Title: **Breakdown of Linear Dielectric Theory for the Interaction between Hydrated Ions and Graphene**

Author(s): Loche, P., Ayaz, C., Schlaich, A., Bonthuis, D. J., & Netz, R. R.

Document type: Postprint

Terms of Use: Copyright applies. A non-exclusive, non-transferable and limited right to use is granted. This document is intended solely for personal, non-commercial use.

Citation: This document is the Accepted Manuscript version of a Published Work that appeared in final form in The Journal of Physical Chemistry Letters, copyright © American Chemical Society after peer review and technical editing by the publisher. To access the final edited and published work see https://doi.org/10.1021/acs.jpclett.8b02473.

Loche, P., Ayaz, C., Schlaich, A., Bonthuis, D. J., & Netz, R. R. (2018). Breakdown of Linear Dielectric Theory for the Interaction between Hydrated Ions and Graphene. The Journal of Physical Chemistry Letters, 9(22), 6463–6468. https://doi.org/10.1021/acs.jpclett.8b02473

Breakdown of linear dielectric theory for the interaction between hydrated ions and graphene

Philip Loche,[†] Cihan Ayaz,[†] Alexander Schlaich,[†,‡] Douwe J. Bonthuis,[†] and Roland R. Netz[*,†]

†Fachbereich Physik, Freie Universität Berlin, Arnimallee 14, 14195 Berlin, Germany
‡Laboratoire Interdisciplinaire de Physique, CNRS and Université Grenoble Alpes, UMR CNRS 5588, 38000 Grenoble, France

Abstract

Many vital processes taking place in electrolytes, such as nanoparticle self-assembly, water purification and the operation of supercapacitors, rely on the precise many-body interactions between surfaces and ions in water. Here we study the interaction between a hydrated ion and a charge-neutral graphene layer using atomistic molecular dynamics simulations. For small separations, the ion-graphene repulsion is of non-electrostatic nature and for intermediate separations Van-der-Waals attraction becomes important. Contrary to prevailing theory, we show that non-linear and tensorial dielectric effects become non-negligible close to surfaces, even for monovalent ions. This breakdown of standard isotropic linear dielectric theory has important consequences for the understanding and modeling of charged objects at surfaces.

Graphical TOC Entry

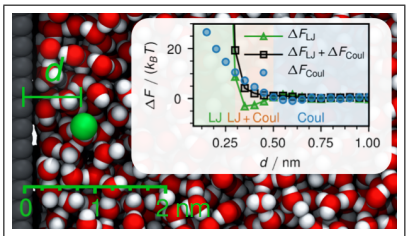

Simulation snapshot of a chloride ion close to a graphene layer; the inset presents the free energy decomposition into electrostatic and non-electrostatic contributions.

The anomalous properties of electrolytes in the vicinity of hydrophobic surfaces have a profound influence on a diverse range of applications, such as graphene-based water purification[1], double-layer capacitance[2] osmotic power harvesting[3] and electrowetting[4], as well as for biological functions, such as molecular recognition[5] and DNA condensation[6]. In the simplest theory, ions are assumed to be point-like and embedded in a structureless, linear dielectric medium. At an interface to a low-dielectric medium the resulting image charge repulsion diverges inversely with the ion-interface separation. For the air-water interface, Onsager and Samaras used these assumptions to derive the ion surface depletion and from that the roughly linear increase in surface tension with salt concentration, in good agreement with experiments[7]. This theory does not account for the ion size and other ion specificities that give rise to Hofmeister effects. In fact, large halide ions such as iodide are slightly less repelled from the air-water interface than small halide ions such as fluoride or chloride, which in experiments leads to ionic-specific differences of electrolyte interfacial tensions in agreement with atomistic simulations that include explicit water[8–11]. Similar ion-specific effects are also present at solid surfaces[12,13]. In coarse-grained models that do not explicitly account for molecular water effects ion-specific effects can be included by adding heuristic ion-surface interactions[14–19]. In alternative approaches the interaction of a finite-size ion with a step-like dielectric boundary was derived from linear dielectric theory[20,21,23] and the ion radius and excess polarizability were estimated from experimental data, yielding good agreement of predicted ionic surface affinities with simulations and experiments[22,24,25].

Yet such heuristic approaches are problematic for a number of reasons: First, the dielectric response of water at interfaces varies with distance and is not isotropic but tensorial and described by significantly different parallel and perpendicular profiles[26]. This becomes particularly important in nano-confinement as recently shown in simulations and experiments[2,27]. Secondly, the electric field produced even by monovalent ions is strong and linear dielectric theory breaks down in the ionic vicinity; how such non-linear effects modify the dielectric interfacial behavior is far from clear. Thirdly, while it is clear that van-der-Waals and steric interactions are present at solid surfaces in addition to dielectric image-charge interactions, the relative magnitude of all these interactions is not known, even though that information is critical for constructing an accurate theory of ion-surface interactions.

Here we determine the free energy profile for a single ion (modeled with chloride Lennard-Jones (LJ) parameters) close to a neutral graphene/water interface. We choose graphene because it is both simple and highly relevant for nanotechnological applications[1,4,28–32]. Note that the graphene surface that we use is hydrophobic, but our results are not necessarily limited to hydrophobic surfaces.

By splitting the ionic free energy into electrostatic and non-electrostatic LJ contributions we show that LJ contributions dominate close to the surface. By thermodynamic integration (TI) we furthermore demonstrate that the non-linear dielectric response becomes significant as the ion approaches the surface. Finally, to accurately describe the linear dielectric contribution to the ion-surface interaction, which only makes up a small fraction of the total interaction, tensorial dielectric theory must be used. Thus simple isotropic linear dielectric theory misses the fundamental physics of ion-surface interactions and the associated parameters require careful interpretation.

We simulate two parallel neutral graphene layers at a fixed separation $L = 9.95\,\mathrm{nm}$ with 8701 SPC/E water molecules using the GROMOS54A7 force field[33] (see Figure 1a for a snapshot), results for the alternative $TIP4P_{\mathrm{EW}}$ water model are shown in the Supplementary Information. All simulation are performed using the 2016 version of the GROMACS simulation package[34]. Figure 1b exhibits the water mass density profile $\rho_m(z)$ with oscillations typical for rigid surfaces. The system contains two ions, the so-called test ion is located at a variable separation d from the carbon atoms forming one graphene sheet while the so-called

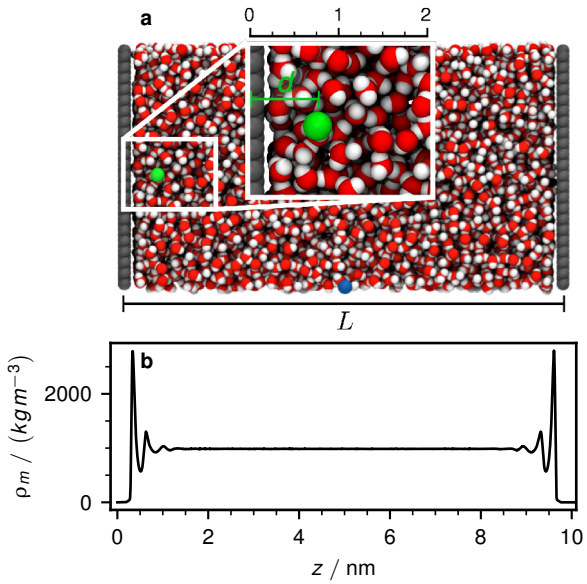

Figure 1: **a** Simulation snapshot showing the two parallel neutral graphene layers at a fixed distance $L = 9.945\,\mathrm{nm}$, SPC/E water molecules, the test ion at a separation $d = 0.75\,\mathrm{nm}$ (green) and the counter ion at fixed position $z = 5\,\mathrm{nm}$ (blue). **b** Water mass density profile.

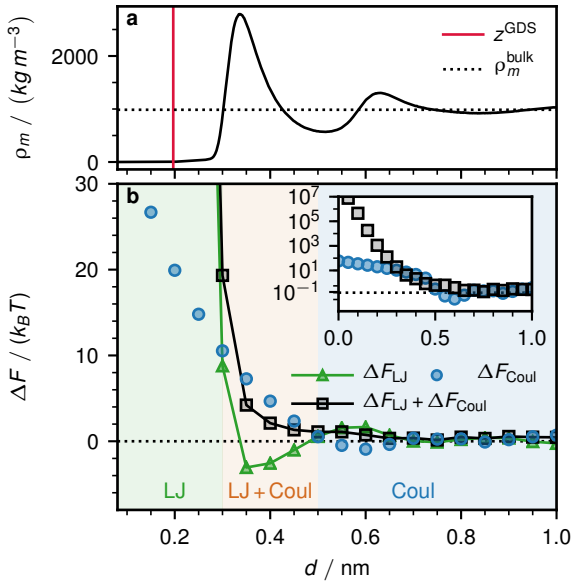

Figure 2: **a** Water mass density profile with Gibbs-dividing surface (GDS) position (red vertical line) and buk density (horizontal dotted line). **b** Ion-graphene interaction free energy $\Delta F(d)$ split into the LJ and Coulomb contributions $\Delta F_{\mathrm{LJ}}(d)$ and $\Delta F_{\mathrm{Coul}}(d)$. The inset shows results on a log scale.

counter ion is fixed in the slab center. The total simulation system is charge neutral to avoid artifacts from the periodic boundary conditions[35]. The LJ parameters of test and counter ions correspond to the chloride force field by Weerasinghe and Smith[36]. During the simulation runs the charge neutral graphene layers and the ions are fixed in space. The d-dependent free energy $F(d)$ is obtained by TI. For each d we first create a neutral LJ cavity and thereby obtain the solvation free energy of a neutral LJ sphere $F_{\mathrm{LJ}}(d)$, followed by a charging procedure which yields the Coulomb free energy contribution $F_{\mathrm{Coul}}(d)$. To obtain the free energy of the test ion, we subtract the solvation energy of the isolated counter ion (from separate bulk simulations) and the analytically calculated electrostatic interaction between test and counter ions (see Supplemental Information for technical details).

Figure 2a shows a magnification of the water mass density profile in the interfacial region, in Figure 2b the ion-surface interaction free energy, obtained by subtracting the solvation free energy in the slab center,

$$\Delta F(d) = F(d) - F(L/2) = \Delta F_{\mathrm{LJ}}(d) + \Delta F_{\mathrm{Coul}}(d), \quad (1)$$

is presented together with its LJ and Coulomb contributions. For reference, the free energy contributions in the slab center are $F_{\mathrm{LJ}}(L/2) = 8.9\,\mathrm{k_B T}$ and $F_{\mathrm{Coul}}(L/2) = -151.1\,\mathrm{k_B T}$, which agree perfectly with simulations in a bulk system (Supplementary Information). The results for the total free energy $\Delta F(d)$ agree with earlier works[12,37]. Our decomposition into LJ and Coulomb parts shows that the LJ contribution completely dominates for small $d < 0.3\,\mathrm{nm}$ and thus at separations considerably larger than the Gibbs-dividing surface (GDS) position at $d \approx 0.2\,\mathrm{nm}$ [red line in Figure 2b]. In the intermediate distance range $0.35\,\mathrm{nm} < d < 0.5\,\mathrm{nm}$ the Coulomb repulsion is significantly weakened by LJ attraction. We conclude that the Coulomb contribution $\Delta F_{\mathrm{Coul}}(d)$ by itself does

not represent the total ion-surface interaction well.

In standard ionic hydration approaches water is modeled as a symmetric linear homogeneous dielectric medium[38], according to which the ionic hydration free energy scales $\propto q^2$ with the ionic valency q (measured in units of the elementary charge). It is well known that since water is charge asymmetric the ionic hydration free energy is also asymmetric with respect to q and in fact favors anion versus cation solvation[39–41]. Moreover, non-linear dielectric contributions have been shown to be significant for ion solvation in bulk[42,43]. We thus introduce a non-linear dielectric model for the Coulomb part of the ion-surface interaction

$$F_{\mathrm{Coul}}(d) = \phi(d)q + A(d)q^2 + B(d)q^3 + C(d)q^4. \quad (2)$$

The potential ϕ primarily accounts for the cation/anion symmetry breaking and reflects the presence of a non-zero electrostatic potential inside a LJ cavity due to water orientation effects. The quadratic coefficient A is the linear dielectric Born coefficient while B and C reflect non-linear dielectric effects. Figure 3a shows F_{Coul} as a function of the ion charge q for several ion-surface separations d (blue symbols) as well as for a single ion in a periodic bulk water box (red symbols). The good agreement between bulk and slab simulations for $d = 1.0\,\mathrm{nm}$ demonstrates that boundary condition effects are properly accounted for in our analysis. All data show the cation/anion asymmetry around $q = 0$[39]. Lines show fits according to eq. (2) (see Supplementary Information for details).

Figure 3b–e presents the separation-dependent dielectric coefficients defined in eq. (2), all rescaled by elementary charge and thermal energy $\mathrm{k_BT}$. The horizontal red dashed lines show bulk results, which agree well with the slab simulations for large d. For the electrostatic potential in the LJ cavity ϕ in Figure 3b we add a Volt scale, in the slab center we obtain $\phi(L/2) = 0.38\,\mathrm{V}$ in agreement with previous bulk simulations[43,46]. At the interface the potential ϕ only changes slightly, whereas the sizable electrostatic potential shows large oscillations and even a different sign, as shown in the Supplemental Information. This means that the sizable electrostatic potential of a planar interface, which in previous works was suggested to influence the interfacial ion transfer[44,45], is largely compensated by the LJ cavity potential. The quadratic coefficient A in Figure 3c denotes the linear dielectric response of water. The relative contribution of the linear to the overall dielectric solvation response is for a monovalent negative ion given by $A/(-\phi+A-B+C)$; far away from the interface, i.e. for large d, we obtain 71 % and can thus say that the linear contribution is dominant. For the Coulomb contribution to the interaction energy, $\Delta F_{\mathrm{Coul}}(d) = F_{\mathrm{Coul}}(d) - F_{\mathrm{Coul}}(L/2)$, we obtain that at the surface ($d = 0$) the relative linear contribution only amounts to 53 %. We conclude that non-linear dielectric effects become significant at surfaces.

We next demonstrate how the linear dielectric contribution Aq^2 in eq. (2) is related to continuum dielectric linear response theory. As we have shown previously, at a planar interface the dielectric response is tensorial and described by perpendicular and parallel dielectric profiles $\varepsilon_\perp(d)$ and $\varepsilon_\parallel(d)$[26], which can be straightforwardly extracted from our simulations and are shown in the Supplementary Information. To arrive at an analytically manageable form, the dielectric profiles can be replaced by step functions of the form $\varepsilon_{\perp/\parallel}(d) = 1$ for $d < z^{\mathrm{DDS}}_{\perp/\parallel}$ and $\varepsilon_{\perp/\parallel}(d) = \varepsilon_{\mathrm{bulk}}$ for $d > z^{\mathrm{DDS}}_{\perp/\parallel}$[26], where the bulk water dielectric constant for SPC/E water is $\varepsilon_{\mathrm{bulk}} = 70$ and the dielectric dividing surface (DDS) positions follow from the dielectric profiles via electrostatic integrability conditions as $z^{\mathrm{DDS}}_\perp = 0.18\,\mathrm{nm}$ and $z^{\mathrm{DDS}}_\parallel = 0.03\,\mathrm{nm}$. We thus see that $z^{\mathrm{DDS}}_\perp > z^{\mathrm{DDS}}_\parallel$, the shift between the DDS is in between the values previously found for diamond[26] and self-assembled surfaces[27]. The coarse-grained dielectric model for the graphene-water interface thus consists of three regions as shown in Figure 4a: $\varepsilon_\perp = \varepsilon_\parallel = 1$ in the half space $z < z^{\mathrm{DDS}}_\parallel$, tensorial dielectric constants $\varepsilon_\perp = 1$ and $\varepsilon_\parallel = \varepsilon_{\mathrm{bulk}}$ in a thin slab defined by $z^{\mathrm{DDS}}_\parallel < z < z^{\mathrm{DDS}}_\perp$, and

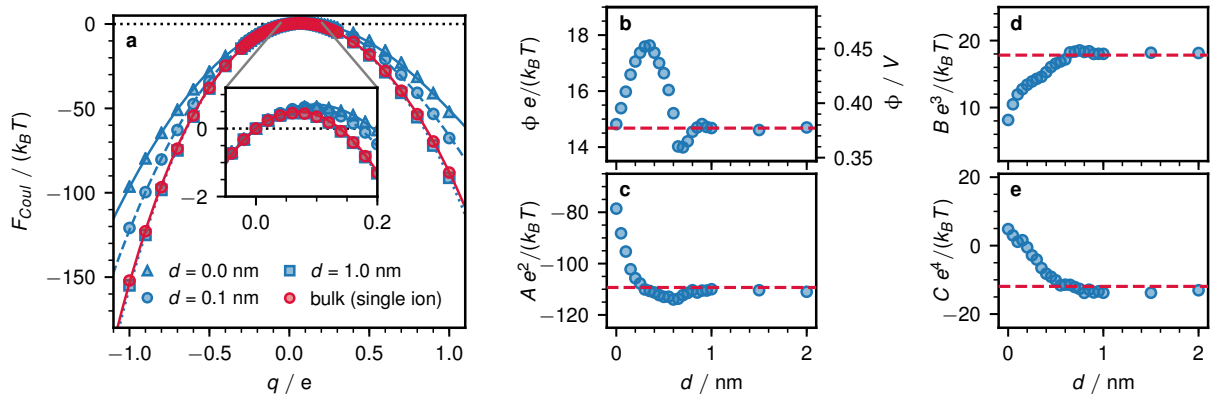

Figure 3: **a** Coulomb part is for different separations from the graphene surface d represented by different blue symbols. Red symbols show results for an ion in a periodic bulk water box. Lines are fits according to eq. (2). **b**–**e** Coefficients are defined in eq. (2) and obtained from fits of the Coulomb solvation contribution shown in a. The horizontal red dashed lines show results for an ion in a periodic bulk water box.

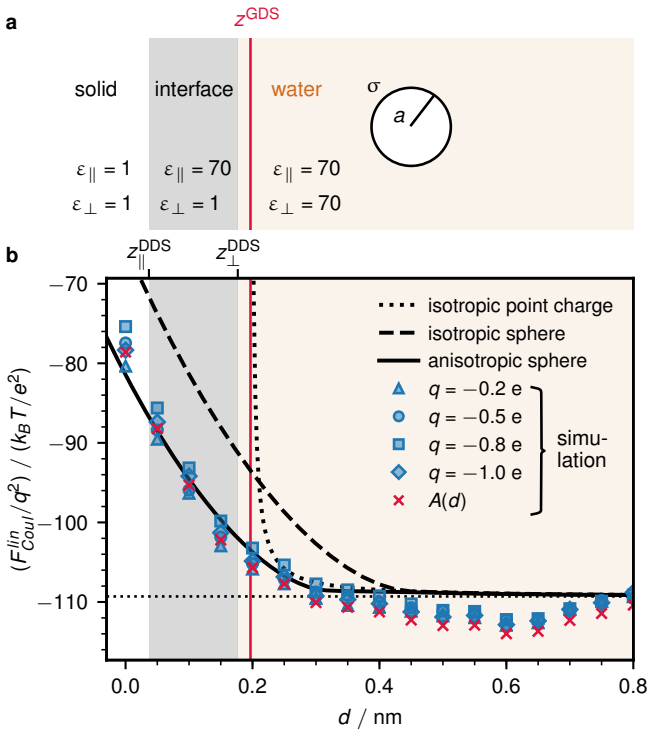

Figure 4: **a** Continuum model for the dielectric interaction of a sphere with radius a and surface charge σ with an interface that exhibits a tensorial dielectric constant for $z_\parallel^{\mathrm{DDS}} < z < z_\perp^{\mathrm{DDS}}$. **b** Rescaled linear dielectric free energy contribution $\Delta F_{\mathrm{Coul}}^{\mathrm{lin}}/q^2$ based on eq. (5). Blue symbols show simulation results, red crosses denote the linear prediction Aq^2 based on eq. (2), lines are different continuum model predictions (see text).

$\varepsilon_\perp = \varepsilon_\parallel = \varepsilon_{\mathrm{bulk}}$ in the half space $z_\perp^{\mathrm{DDS}} < z$.

Within linear response theory, the Coulomb free energy associated with a charge density $\rho(\boldsymbol{r})$ is given by

$$F_{\mathrm{Coul}}^{\mathrm{lin}} = \frac{1}{2}\iint \rho(\mathbf{r})\mathcal{G}(\mathbf{r},\mathbf{r}')\rho(\mathbf{r}')\mathrm{d}\mathbf{r}\,\mathrm{d}\mathbf{r}'\,. \qquad (3)$$

The Green's function $\mathcal{G}$ follows from the Poisson equation

$$\varepsilon_0\left\{\nabla\cdot[\hat{\boldsymbol{\varepsilon}}(\mathbf{r})\cdot\nabla\mathcal{G}(\mathbf{r},\mathbf{r}')]\right\} = -\delta(\mathbf{r}-\mathbf{r}')\,, \qquad (4)$$

where the anisotropic permittivity tensor $\hat{\boldsymbol{\varepsilon}}(\mathbf{r})$ is diagonal and piecewise constant in the three regions as defined in Figure 4a. The derivation of $\mathcal{G}$ is explicitly shown in the Supplementary Information.

We model the ion as a sphere with radius a and surface charge density $\sigma = q/4\pi a^2$, yielding a total charge of q, so that the charge distribution of an ion centered at position $\mathbf{r}_0$ is $\rho(\mathbf{r}) = \sigma\delta(|\mathbf{r}-\mathbf{r}_0|-a)$. Inside the sphere we assume the dielectric constant to be same as in the surrounding medium, so that we can use eq. (3) to calculate the electrostatic energy. In the Supplementary Information we show by numerically solving the Poisson equation that using a fixed dielectric constant $\varepsilon = 1$ inside the ion, the dielectric energy is very similar to the results of eq. (3).

The ion radius a we determine by comparing Born's result for the dielectric hydration free energy of a charged spherical shell in bulk[47] $F_{\mathrm{Born}} = q^2(\varepsilon_{\mathrm{bulk}}^{-1} - 1)/(8\pi\varepsilon_0 a)$ with the linear contribution of the simulated Coulomb free energy

$$F_{\mathrm{Coul}}^{\mathrm{lin}}(d) = F_{\mathrm{Coul}}(d) - \phi(d)q - B(d)q^3 - C(d)q^4. \quad (5)$$

For a chloride ion with $q = -1$ and in bulk for $d = L/2$ we obtain $F_{\mathrm{Coul}}^{\mathrm{lin}} = -108.9\,\mathrm{k_BT}$, which gives an effective radius of $a = 0.254\,\mathrm{nm}$. This radius is significantly larger than the Pauling crystal radius for chloride, 0.18 nm[48], and also larger than the radius obtained from associating the Born expression with the experimental $F = -142.1\,\mathrm{k_BT}$ or the simulated total chloride hydration free energy $F = -142.2\,\mathrm{k_BT}$, which both yield a radius of 0.19 nm[40]. This is not surprising, since the total hydration free energy contains non-electrostatic as well as non-linear electrostatic contributions, which are not captured by the Born expression F_{Born} and therefore should not be included in a comparison of F_{Born} with hydration energies. The good agreement between the crystal radius and the fitted radii when using the total hydration free energy is purely coincidental and thus unphysical.

Figure 4b compares simulation results for the linear dielectric contribution according to eq. (5) for a few different values of q (open symbols) with the Green's function result defined in eq. (3) (solid line). The agreement is excellent without any fitting parameters and shows that the tensorial dielectric coarse-grained model describes the linear dielectric free energy contribution very well. Note that in Figure 4b all energies are rescaled by the ion charge squared, q^2, in order to eliminate the trivial quadratic charge dependence. We also show the linear coefficient $A(d)$ taken from Figure 3b (red crosses) and again find good agreement, which reconfirms that the non-linear expansion of the dielectric response in eq. (2) is robust. We also compare with dielectric theories that neglect the tensorial character and instead use an isotropic dielectric profile with a jump located at the Gibbs dividing surface (whose location $z^{\mathrm{GDS}} = 0.19\,\mathrm{nm}$ is indicated by a red vertical line in Figure 4). The dotted line shows the free energy for a point charge, which corresponds to the simple image-charge construction and which diverges as the GDS is approached. The dashed line shows the free energy for a charged sphere of finite radius calculated previously[21]; note that this calculation corrected an error in a previous publication[20]. It is seen that the finite-size sphere result for an isotropic dielectric model (broken line) is shifted away from the interface compared to the tensorial model. The divergence of the point-charge model is clearly not present in the simulation data, but this model agrees quite well with the simulation data further away from the interface. This agreement again stems from the cancellation of two errors, namely the neglect of the finite ion size and the wrong positioning of the dielectric dividing surface at the GDS, and thus is not a robust feature of such a simplified model description.

In summary, the interaction of a hydrated ion with a neutral hydrophobic graphene surface is dominated by LJ interactions at small separation, while the Coulombic contribution (which is of dielectric nature) contains significant non-linear contributions. In order to accurately describe the linear contribution to the dielectric ion-surface interaction, finite ion size and tensorial interfacial dielectric effects must be taken into account. The failure of standard linear dielectric theory at interfaces is typically hidden by a subtle cancelation of errors due to using an unphysical ion size, the neglect of tensorial and non-linear dielectric effects and the neglect of non-electrostatic forces. Finally, our results show that generalizing the Poisson-Boltzmann approach to electrolyte interfaces by including non-electrostatic ion-surface interactions, as has become widespread practice in recent years[12,18,49,50], is meaningful.

Acknowledgement This work was supported by the Deutsche Forschungsgemeinschaft within a grant from Sonderforschungsbereich (SFB) 765 and by grant NE 810/11.

Supporting Information Available

The following files are available free of charge.

- imagecharge_si.pdf: Contains details on the simulation methods, a comparison with a different water model and the analytical and numerical solutions of the tensorial Poisson equation.

References

(1) Chen, L.; Shi, G.; Shen, J.; Peng, B.; Zhang, B.; Wang, Y.; Bian, F.; Wang, J.; Li, D.; Qian, Z. et al. Ion sieving in graphene oxide membranes via cationic control of interlayer spacing. *Nature* **2017**, *550*, 380–383.

(2) Fumagalli, L.; Esfandiar, A.; Fabregas, R.; Hu, S.; Ares, P.; Janardanan, A.; Yang, Q.; Radha, B.; Taniguchi, T.; Watanabe, K. et al. Anomalously low dielectric constant of confined water. *Science* **2018**, *360*, 1339–1342.

(3) Siria, A.; Bocquet, M.-L.; Bocquet, L. New avenues for the large-scale harvesting of blue energy. *Nature Reviews Chemistry* **2017**, *1*, 0091.

(4) Tabassian, R.; Oh, J.-H.; Kim, S.; Kim, D.; Ryu, S.; Cho, S.-M.; Koratkar, N.; Oh, I.-K. Graphene-coated meshes for electroactive flow control devices utilizing two antagonistic functions of repellency and permeability. *Nature Communications* **2016**, *7*, 13345.

(5) Ma, C. D.; Wang, C.; Acevedo-Vélez, C.; Gellman, S. H.; Abbott, N. L. Modulation of hydrophobic interactions by proximally immobilized ions. *Nature* **2015**, *517*, 347–350.

(6) Besteman, K.; Eijk, K. V.; Lemay, S. G. Charge inversion accompanies DNA condensation by multivalent ions. *Nature Physics* **2007**, *3*, 641–644.

(7) Onsager, L.; Samaras, N. N. T. The Surface Tension of Debye-Hückel Electrolytes. *The Journal of Chemical Physics* **1934**, *2*, 528–536.

(8) Jungwirth, P.; Tobias, D. J. Specific Ion Effects at the Air/Water Interface. *Chemical Reviews* **2006**, *106*, 1259–1281.

(9) Ghosal, S.; Hemminger, J. C.; Bluhm, H.; Mun, B. S.; Hebenstreit, E. L. D.; Ketteler, G.; Ogletree, D. F.; Requejo, F. G.; Salmeron, M. Electron Spectroscopy of Aqueous Solution Interfaces Reveals Surface Enhancement of Halides. *Science* **2005**, *307*, 563–566.

(10) Horinek, D.; Herz, A.; Vrbka, L.; Sedlmeier, F.; Mamatkulov, S. I.; Netz, R. R. Specific ion adsorption at the air/water interface: The role of hydrophobic solvation. *Chemical Physics Letters* **2009**, *479*, 173–183.

(11) Noah-Vanhoucke, J.; Geissler, P. L. On the fluctuations that drive small ions toward, and away from, interfaces between polar liquids and their vapors. *Proceedings of the National Academy of Sciences* **2009**, *106*, 15125–15130.

(12) Horinek, D.; Serr, A.; Bonthuis, D. J.; Boström, M.; Kunz, W.; Netz, R. R. Molecular Hydrophobic Attraction and Ion-Specific Effects Studied by Molecular Dynamics. *Langmuir* **2008**, *24*, 1271–1283.

(13) Lund, M.; Vácha, R.; Jungwirth, P. Specific Ion Binding to Macromolecules: Effects of Hydrophobicity and Ion Pairing. *Langmuir* **2008**, *24*, 3387–3391.

(14) Markovich, T.; Andelman, D.; Podgornik, R. Surface tension of electrolyte solutions: A self-consistent theory. *EPL (Europhysics Letters)* **2014**, *106*, 16002.

(15) Manciu, M.; Ruckenstein, E. Specific ion effects via ion hydration: I. Surface tension. *Advances in Colloid and Interface Science* **2003**, *105*, 63–101.

(16) Pegram, L. M.; Record, M. T. Hofmeister Salt Effects on Surface Tension Arise from Partitioning of Anions and Cations between Bulk Water and the Air-Water Interface. *The Journal of Physical Chemistry B* **2007**, *111*, 5411–5417.

(17) Onuki, A. Surface tension of electrolytes: Hydrophilic and hydrophobic ions near an interface. *The Journal of Chemical Physics* **2008**, *128*, 224704.

(18) Schwierz, N.; Netz, R. R. Effective Interaction between Two Ion-Adsorbing Plates: Hofmeister Series and Salting-In/Salting-Out Phase Diagrams from a Global Mean-Field Analysis. *Langmuir* **2012**, *28*, 3881–3886.

(19) Bonthuis, D. J.; Netz, R. R. Unraveling the Combined Effects of Dielectric and Viscosity Profiles on Surface Capacitance, Electro-Osmotic Mobility, and Electric Surface Conductivity. *Langmuir* **2012**, *28*, 16049–16059.

(20) Kharkats, Y. I.; Ulstrup, J. The electrostatic Gibbs energy of finite-size ions near a planar boundary between two dielectric media. *Journal of Electroanalytical Chemistry and Interfacial Electrochemistry* **1991**, *308*, 17–26.

(21) Tamashiro, M. N.; Constantino, M. A. Ions at the Water-Vapor Interface. *The Journal of Physical Chemistry B* **2010**, *114*, 3583–3591.

(22) Levin, Y.; dos Santos, A. P.; Diehl, A. Ions at the Air-Water Interface: An End to a Hundred-Year-Old Mystery? *Physical Review Letters* **2009**, *103*, 257802.

(23) Wang, R.; Wang, Z.-G. Continuous Self-Energy of Ions at the Dielectric Interface. *Physical Review Letters* **2014**, *112*, 136101.

(24) dos Santos, A. P.; Diehl, A.; Levin, Y. Surface Tensions, Surface Potentials, and the Hofmeister Series of Electrolyte Solutions. *Langmuir* **2010**, *26*, 10778–10783.

(25) Levin, Y.; dos Santos, A. P. Ions at hydrophobic interfaces. *Journal of Physics: Condensed Matter* **2014**, *26*, 203101.

(26) Bonthuis, D. J.; Gekle, S.; Netz, R. R. Profile of the static permittivity tensor of water at interfaces: consequences for capacitance, hydration interaction and ion adsorption. *Langmuir: the ACS journal of surfaces and colloids* **2012**, *28*, 7679–7694.

(27) Schlaich, A.; Knapp, E. W.; Netz, R. R. Water Dielectric Effects in Planar Confinement. *Physical Review Letters* **2016**, *117*, 048001.

(28) Novoselov, K. S.; Fal'ko, V. I.; Colombo, L.; Gellert, P. R.; Schwab, M. G.; Kim, K. A roadmap for graphene. *Nature* **2012**, *490*, 192.

(29) Stoller, M. D.; Park, S.; Zhu, Y.; An, J.; Ruoff, R. S. Graphene-Based Ultracapacitors. *Nano Letters* **2008**, *8*, 3498–3502.

(30) Joshi, R. K.; Carbone, P.; Wang, F. C.; Kravets, V. G.; Su, Y.; Grigorieva, I. V.; Wu, H. A.; Geim, A. K.; Nair, R. R. Precise and Ultrafast Molecular Sieving Through Graphene Oxide Membranes. *Science* **2014**, *343*, 752–754.

(31) Gravelle, S.; Yoshida, H.; Joly, L.; Ybert, C.; Bocquet, L. Carbon membranes for efficient water-ethanol separation. *The Journal of Chemical Physics* **2016**, *145*, 124708.

(32) Akbari, A.; Sheath, P.; Martin, S. T.; Shinde, D. B.; Shaibani, M.; Banerjee, P. C.; Tkacz, R.; Bhattacharyya, D.; Majumder, M. Large-area graphene-based nanofiltration membranes by shear alignment of discotic nematic liquid crystals of graphene oxide. *Nature Communications* **2016**, *7*, 10891.

(33) Schmid, N.; Eichenberger, A. P.; Choutko, A.; Riniker, S.; Winger, M.; Mark, A. E.; Gunsteren, W. F. v. Definition and testing of the GROMOS

force-field versions 54A7 and 54B7. *European Biophysics Journal* **2011**, *40*, 843.

(34) Abraham, M. J.; Murtola, T.; Schulz, R.; Páll, S.; Smith, J. C.; Hess, B.; Lindahl, E. GROMACS: High performance molecular simulations through multi-level parallelism from laptops to supercomputers. *SoftwareX* **2015**, *1-2*, 19–25.

(35) Hub, J. S.; de Groot, B. L.; Grubmüller, H.; Groenhof, G. Quantifying Artifacts in Ewald Simulations of Inhomogeneous Systems with a Net Charge. *Journal of Chemical Theory and Computation* **2014**, *10*, 381–390.

(36) Weerasinghe, S.; Smith, P. E. A Kirkwood–Buff derived force field for sodium chloride in water. *The Journal of Chemical Physics* **2003**, *119*, 11342–11349.

(37) Rotenberg, B.; Marry, V.; Vuilleumier, R.; Malikova, N.; Simon, C.; Turq, P. Water and ions in clays: Unraveling the interlayer/micropore exchange using molecular dynamics. *Geochimica et Cosmochimica Acta* **2007**, *71*, 5089–5101.

(38) Fröhlich, H. *Theory of Dielectrics: Dielectric Constant and Dielectric Loss*; Oxford University Press, 1987.

(39) Lynden-Bell, R. M.; Rasaiah, J. C. From hydrophobic to hydrophilic behaviour: A simulation study of solvation entropy and free energy of simple solutes. *The Journal of Chemical Physics* **1997**, *107*, 1981–1991.

(40) Latimer, W. M.; Pitzer, K. S.; Slansky, C. M. The Free Energy of Hydration of Gaseous Ions, and the Absolute Potential of the Normal Calomel Electrode. *The Journal of Chemical Physics* **1939**, *7*, 108–111.

(41) Rashin, A. A.; Honig, B. Reevaluation of the Born model of ion hydration. *The Journal of Physical Chemistry* **1985**, *89*, 5588–5593.

(42) Rajamani, S.; Ghosh, T.; Garde, S. Size dependent ion hydration, its asymmetry, and convergence to macroscopic behavior. *The Journal of Chemical Physics* **2004**, *120*, 4457–4466.

(43) Bardhan, J. P.; Jungwirth, P.; Makowski, L. Affine-response model of molecular solvation of ions: Accurate predictions of asymmetric charging free energies. *The Journal of Chemical Physics* **2012**, *137*.

(44) Horinek, D.; Netz, R. R. Specific Ion Adsorption at Hydrophobic Solid Surfaces. *Physical Review Letters* **2007**, *99*, 226104.

(45) Baer, M. D.; Stern, A. C.; Levin, Y.; Tobias, D. J.; Mundy, C. J. Electrochemical Surface Potential Due to Classical Point Charge Models Drives Anion Adsorption to the Air–Water Interface. *The Journal of Physical Chemistry Letters* **2012**, *3*, 1565–1570.

(46) Ashbaugh, H. S. Convergence of Molecular and Macroscopic Continuum Descriptions of Ion Hydration. *The Journal of Physical Chemistry B* **2000**, *104*, 7235–7238.

(47) Born, M. Volumen und Hydratationswärme der Ionen. *Zeitschrift für Physik* **1920**, *1*, 45–48.

(48) Pauling, L. *The Nature of the Chemical Bond and the Structure of Molecules and Crystals: An Introduction to Modern Structural Chemistry*; Cornell University Press, 1960.

(49) Luo, G.; Malkova, S.; Yoon, J.; Schultz, D. G.; Lin, B.; Meron, M.; Benjamin, I.; Vanýsek, P.; Schlossman, M. L. Ion Distributions near a Liquid-Liquid Interface. *Science* **2006**, *311*, 216–218.

(50) Uematsu, Y.; Bonthuis, D. J.; Netz, R. R. Charged Surface-Active Impurities at Nanomolar Concentration Induce Jones–Ray Effect. *The Journal of Physical Chemistry Letters* **2018**, *9*, 189–193.